A Dynamic Nuclear Magnetic Resonance Study of Trimethylplatinum(IV) Halide Complexes of 1,1,2,2-Tetrakis(methylthio)ethane. Part 1. Low-temperature Solution Properties, and *X*-Ray Crystal Structure of $[PtIMe_3\{(MeS)_2CHCH(SMe)_2\}]$†

Edward W. Abel, Timothy P. J. Coston, Kevin M. Higgins, Keith G. Orrell,* and Vladimir Šik
Department of Chemistry, The University, Exeter EX4 4QD
T. Stanley Cameron
Department of Chemistry, Dalhousie University, Halifax B3 3J3, Canada

Trimethylplatinum(IV) halides $[(PtXMe_3)_4]$ react with equimolar amounts of the ligand $(MeS)_2CHCH(SMe)_2$(L) to give chelate complexes of type $[PtXMe_3L]$ as major products and dinuclear complexes $[(PtXMe_3)_2L]$ as minor components. The chelate complexes in $CDCl_3$ solution exist as *cis* and *trans* configurational isomers, with the *trans* predominating. At temperatures below *ca.* −30 °C, pyramidal inversion of the co-ordinated S atoms is slow on the ^1H and ^{195}Pt time-scales and six invertomer species (*viz.* *trans*/DL-1,2,3, and 4 and *cis*-1/*meso*-1 and DL) have been detected, identified, and characterised by ^1H and ^{195}Pt n.m.r. spectroscopy. The pyramidal inversion rates and energies of the co-ordinated S atom pairs in all six invertomers have been quantitatively measured by a combination of ^1H bandshape analysis and ^{195}Pt two-dimensional EXSY experiments. The resulting $\Delta G^{\ddagger}$ (298.15 K) values lie in the range 54—65 kJ mol^{-1} and are governed primarily by the orientation of the contiguous unco-ordinated S-methyl group. The *X*-ray crystal structure of $[PtIMe_3\{(MeS)_2CHCH(SMe)_2\}]$ depicts the ligand with its co-ordinated S-methyls *trans* to each other and *trans* to their contiguous unco-ordinated S-methyls. This structure corresponds to the most populous $CDCl_3$ solution invertomer (*trans*/DL-2).

Bridge-cleavage reactions of trimethylplatinum(IV) halide tetramers $[(PtXMe_3)_4]$ (X = Cl, Br, or I) with dithio- and diseleno-ethers, $MeE(CH_2)_nEMe$ (E = S or Se), have been extensively studied.[1,2] When n = 2 or 3, mononuclear chelate complexes of formula $[PtXMe_3\{MeE(CH_2)_nEMe\}]$ are formed,[3,4] whereas when n = 0 or 1, halogen-bridged dinuclear complexes of type $[(PtXMe_3)_2\{MeE(CH_2)_nEMe\}]$ are the exclusive products.[5-7] Thus, the principal factor determining whether mononuclear or dinuclear complexes are formed appears to be the number of carbon atoms between the potential donor sites. Recently, the ligand tris(methylthio)-methane, $HC(SMe)_3$, was found to conform to this pattern by producing only dinuclear complexes $[(PtXMe_3)_2\{HC(SMe)_3\}]$.[8]

As an extension to this work, the co-ordination of poly-(organosulphur) ligands to trimethylplatinum(IV) halides has now been investigated. Several reports have appeared[9-11] of complexes with the stable ligand 1,1,2,2-tetrakis(methylthio)-ethene, $(MeS)_2C{=}C(SMe)_2$, but very few complexes of poly-(organosulphur)ethanes have been reported. Attention was therefore directed towards 1,1,2,2-tetrakis(methylthio)ethane, $(MeS)_2CHCH(SMe)_2$, and hexakis(methylthio)ethane, $(MeS)_3CC(SMe)_3$. While the latter ligand has been reported previously,[12] it is extremely moisture-sensitive and difficult to isolate pure. It was therefore not pursued further. Little is known regarding the co-ordination properties of $(MeS)_2CHCH(SMe)_2$(L) apart from a recent report of a chromium(0) tetracarbonyl complex $[Cr(CO)_4\{(MeS)_2CHCH(SMe)_2\}]$.[13] This ligand has interesting metal co-ordination possibilities as it possesses the alternatives of either one or two carbon atoms between its sulphur donors. Thus, mononuclear complexes of type $[PtXMe_3L]$ (**1**) halogen- or ligand-bridged dinuclear complexes of type $[(PtXMe_3)_2L]$ (**2**) and (**3**), and tetranuclear complexes of type $[(PtXMe_3)_4L]$ (**4**) can all be envisaged (Figure 1).

This paper describes the isolation of complexes (**1**) as the predominant products of mixing equimolar quantities of $[PtXMe_3]$ and L, the *X*-ray crystal structure of $[PtIMe_3L]$, and the characterisation of all three halide complexes in $CDCl_3$ solution by ^1H and ^{195}Pt n.m.r. spectra measured in the low-temperature range, ambient to *ca.* −60 °C, over which the effects of pyramidal inversions of the co-ordinated sulphurs are apparent. A subsequent paper will describe the fluxional properties of these complexes in the above-ambient temperature range.

Experimental

Materials.—The ligand 1,1,2,2-tetrakis(methylthio)ethane, $(MeS)_2CHCH(SMe)_2$ was prepared as described previously.[13] The three halogen complexes $[PtXMe_3\{(MeS)_2CHCH(SMe)_2\}]$ (X = Cl, Br, or I) were prepared in an analogous way. The case of X = Cl will be described. A slight excess of ligand (0.16 g, 0.746 mmol) in chloroform (3 cm^3) was added to trimethylplatinum(IV) chloride (0.20 g, 0.725 mmol‡) in chloroform (5 cm^3) and the resulting solution refluxed for 3 h. The solvent was then removed under reduced pressure and the resulting yellow residue recrystallised from dichloromethane–hexane as white crystals of chlorotrimethyl[1,1,2,2-tetrakis-(methylthio)ethane]platinum(IV), m.p. 154.2—156.5 °C; yield 0.34 g, 95.6%. Analytical data (Butterworth Laboratories, London) for all three complexes are given in Table 1.

N.M.R. Spectra.—All ^1H and ^{195}Pt spectra were recorded on a Bruker AM250 F. T. spectrometer operating at 250.13 and

† Iodotrimethyl[1,1,2,2-tetrakis(methylthio)ethane-*SS*′]platinum.

Supplementary data available: see Instructions for Authors, *J. Chem. Soc., Dalton Trans.*, 1989, Issue 1, pp. xvii–xx.

‡ Molar amount based on the monomeric unit, $PtXMe_3$.

Table 1. Analytical data for the mononuclear complexes $[PtXMe_3L]$

Compound	Colour	Yield (%)	M.p./°C	Analysis*/% C	H
$(MeS)_2CHCH(SMe)_2$(L)	White		59—60	33.65 (33.60)	6.65 (6.60)
$[PtClMe_3L]$	White	95.6	154—156	22.10 (22.05)	4.85 (4.75)
$[PtBrMe_3L]$	Off-white	69.3	146—148	20.20 (20.20)	4.00 (4.35)
$[PtIMe_3L]$	Light brown	74.6	169—175	18.45 (18.40)	3.90 (4.00)

* Calculated values in parentheses.

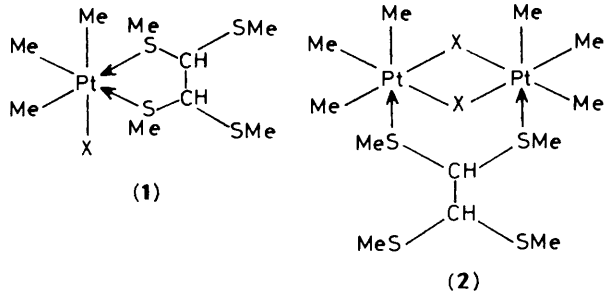

(1) (2)

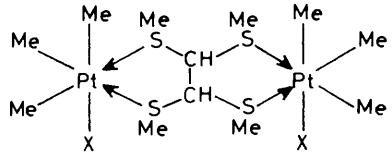

(3)

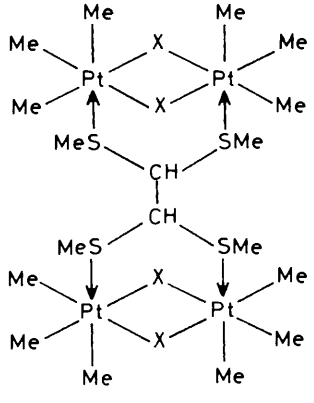

(4)

Figure 1. Possible mononuclear and dinuclear complexes formed from the co-ordination of tetrakis(methylthio)ethane with trimethylplatinum(IV) halides

53.53 MHz respectively. A standard variable-temperature unit was used to control the probe temperature. Samples were maintained at the required temperature for at least 5 min to allow for temperature equilibration before radio frequency (r.f.) pulsing commenced. The probe temperature was checked periodically by a thermocouple to ensure temperature readings were within ±1 °C. Hydrogen-1 chemical shifts are quoted relative to $SiMe_4$ and platinum-195 shifts relative to $\Xi(^{195}Pt)$ =

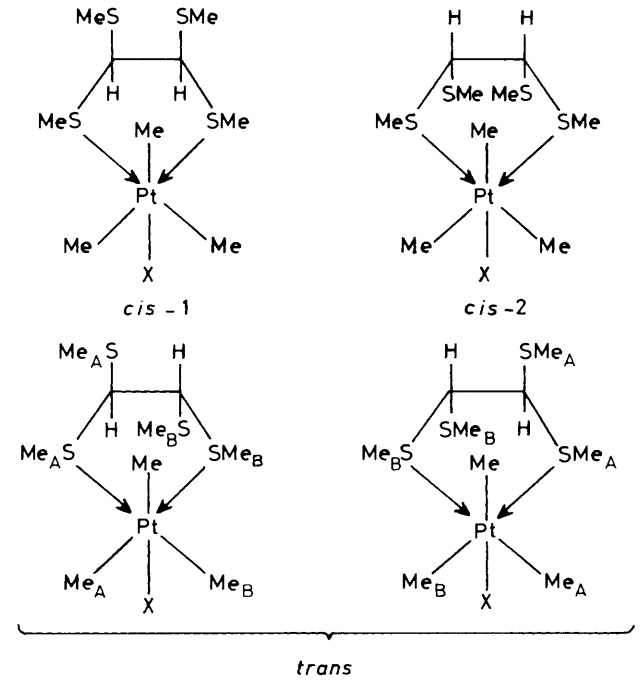

cis -1 *cis* -2

trans

Figure 2. Configurational isomers of $[PtXMe_3\{(MeS)_2CHCH(SMe)_2\}]$

21.4 MHz. All the complexes were studied in [^{2}H]chloroform solution.

Total bandshape analyses were performed with the authors' modified versions of the DNMR3 program.[14] Two-dimensional hydrogen-1 correlation spectroscopy (COSY) and hydrogen-1 and platinum-195 exchange spectroscopy (EXSY) were performed with the Bruker automation programs COSY, NOESY, and NOESYX, respectively. For the EXSY experiments, the mixing times, τ_m, were varied according to the experimental conditions, but in most cases a value of 1 s was found to give the optimum balance of diagonal and off-diagonal signal intensities.[15] Platinum-195 two-dimensional EXSY spectra were based on an F_1 dimension of 128 words, zero-filled to 512 words, and an F_2 dimension of 1 024 words. The number of scans per experiment was in the range 72—184, resulting in an experimental time of *ca.* 16 h. The data were processed using an unshifted sine-bell function in both dimensions. For ^{1}H two-dimensional EXSY spectra the F_1 dimension contained 64 words, zero-filled to 512 words, and the F_2 dimension 1 024 words. Four, eight, or sixteen scans per experiment were employed, depending on the solubility of the complex, giving total experimental times of *ca.* 1—4 h. No window functions were used to process the data on account of the slight exchange broadening present. In all cases, symmetrised, magnitude-mode spectra were calculated.

X-Ray Crystal Data.—$C_9H_{23}IPtS_4$, M = 581.42, monoclinic, a = 7.355(1), b = 15.972(2), c = 14.747(3) Å, β = 99.03(2)°, space group $P2_1/n$, Z = 4, D_c = 2.257 g cm^{-3}, Mo-K_α radiation, λ = 0.7093 Å, μ = 10.0 mm^{-1}.

2 021 Independent observable reflections with $F_o > 2\sigma(F_o)$ were collected on a Nonius CAD4 four-circle diffractometer from a crystal with dimensions 0.1 × 0.2 × 0.25 mm. No absorption corrections were applied. The structure was solved by Patterson and Fourier methods and refined by blocked full-matrix least squares, minimising $\Sigma w\Delta F^2$, where w = $0.325/[\sigma^2(F_o) + 0.0004F_o^2]$. Hydrogen atoms were placed in chemically reasonable positions and were not refined. The final

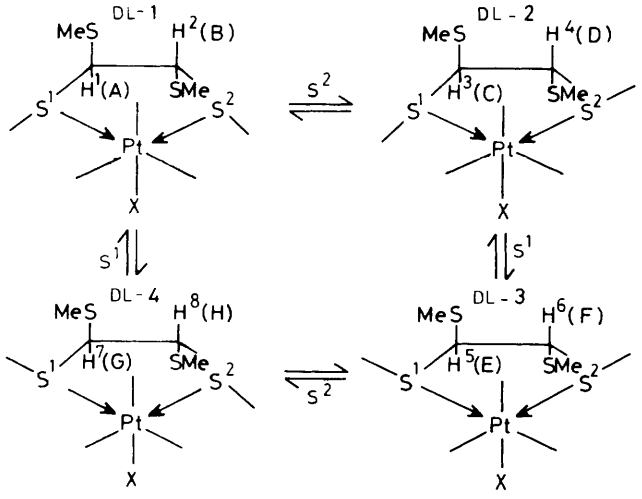

Figure 3. Conformational isomers of the *trans* configuration of [PtX-Me_3\{$(MeS)_2CHCH(SMe)_2$\}] showing the methine proton labelling

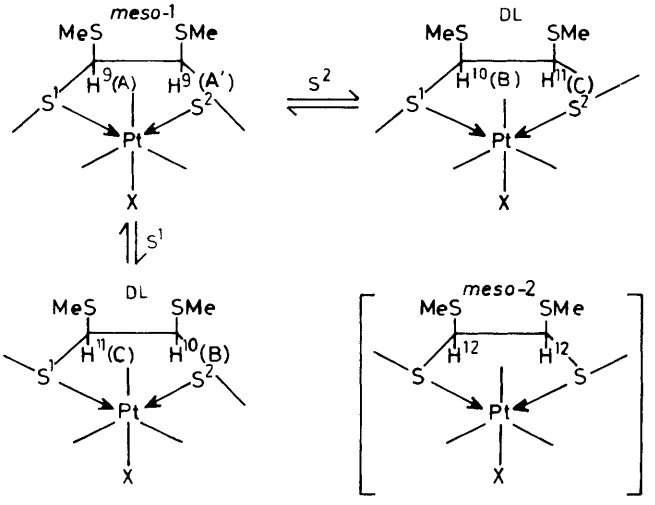

Figure 4. Conformational isomers of the *cis*-1 configuration of [PtX-Me_3\{$(MeS)_2CHCH(SMe)_2$\}] showing the methine proton labelling

R index (for observable reflections) was 0.079, the program SHELX 76[16] being used for the structure solution and refinement.

Results

The analytical data in Table 1 are consistent with mononuclear, five-membered ring chelate complexes, [$PtXMe_3L$] [type (**1**), Figure 1]. No evidence for halogen-bridged dinuclear complexes [types (**2**) and (**4**), Figure 1] was obtained. However, there is n.m.r. evidence for the ligand-bridged dinuclear complex (**3**) existing in $CDCl_3$ solution in low abundance.

Static N.M.R. Data.—The chiral nature of the ligand backbone carbons in these chelate complexes gives rise to a diastereomeric mixture of species. The configurational isomers are labelled *cis*-1, *cis*-2, and *trans*, according to the relative dispositions of the unco-ordinated S-methyls (Figure 2). The *trans* isomers form a degenerate enantiomeric pair which are n.m.r.-indistinguishable in normal solvents. At low temperatures where sulphur inversion is slow, each configurational

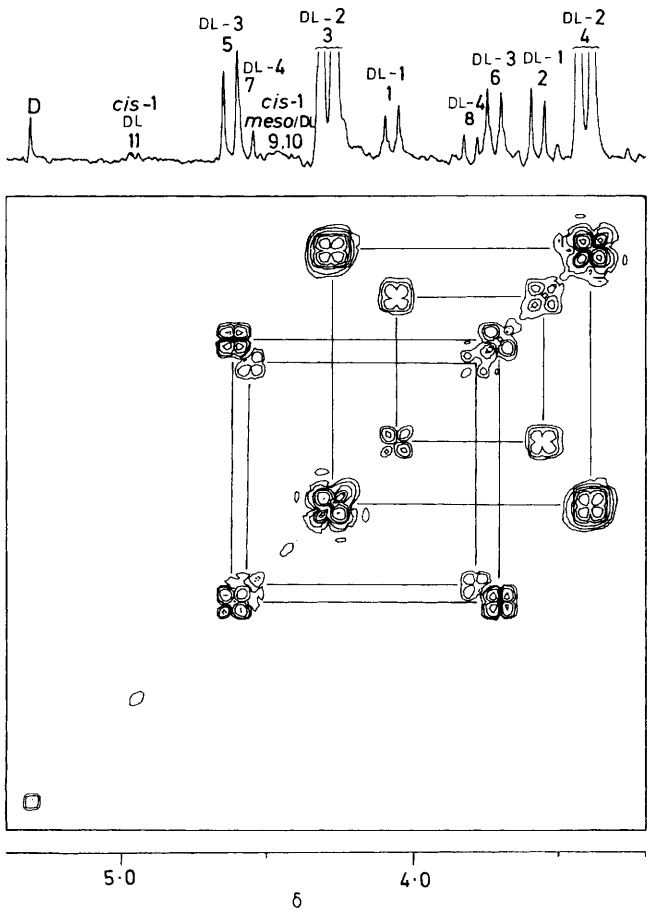

Figure 5. Hydrogen-1 two dimensional COSY spectrum of the methine protons of [$PtIMe_3$\{$(MeS)_2CHCH(SMe)_2$\}] at 213 K. The one-dimensional spectrum shows the band assignments. Numbers refer to Figures 3 and 4; D = dinuclear complex

isomer can exist as a mixture of conformational isomers (invertomers) as shown in Figures 3 and 4 for the *trans* and *cis*-1 isomers (the case of *cis*-2 is not shown for reasons apparent later). Thus *cis*-1 can exist as two *meso* invertomers and a DL pair, and *trans* can exist as four distinct DL pairs, only single members of which are shown. Thus, up to seven solution species are capable of being distinguished by solution n.m.r. spectroscopy at low temperatures.

Hydrogen-1 signals were detected in the regions δ 4—5 (methine protons), 2—3 (co-ordinated and unco-ordinated S-methyls), and 0.5—1.5 (Pt-methyls, *trans* X or *trans* S).

Methine region. This proved most informative and the spectrum of [$PtIMe_3$\{$(MeS)_2CHCH(SMe)_2$\}] at 213 K is shown at the top of Figure 5. At this low temperature, five almost first-order AB quartets, a broad, unresolved signal and an additional signal (labelled D in Figure 5) were identified. Further insight into the assignment of these signals was achieved from a ^1H two dimensional COSY experiment (Figure 5). The high- and low-frequency components of four out of the five AB quartets were identified in this experiment. The fifth quartet with the smaller scalar coupling was too weak. A proton two-dimensional EXSY spectrum obtained at the same temperature showed certain exchange features and indicated that at least two configurational isomers were present. More precise information was derived from ^{195}Pt spectra. The one- and two-dimensional EXSY spectra of the iodo complex at 233

Table 2. Platinum-195 shifts and invertomer populations for $[PtXMe_3\{(MeS)_2CHCH(SMe)_2\}]$ (X = Cl, Br, or I) at 243 K

		δ*			Population (%)		
Configuration	Invertomer	Cl	Br	I	Cl	Br	I
trans	DL-1	1 335.0	1 238.2	1 058.0	27.9	20.4	12.9
	DL-2	1 292.2	1 178.7	981.2	34.5	46.7	55.2
	DL-3	1 289.5	1 152.6	919.9	4.8	8.5	12.8
	DL-4	1 321.8	1 202.7	991.8	4.4	4.7	7.1
cis-1	*meso*-1	1 368.9	1 280.0	1 120.0	25.3	17.4	8.3
	DL	1 368.8	1 252.8	1 051.7	*ca.* 2	2.3	3.7

* Relative to $\Xi(^{195}Pt)$ = 21.4 MHz.

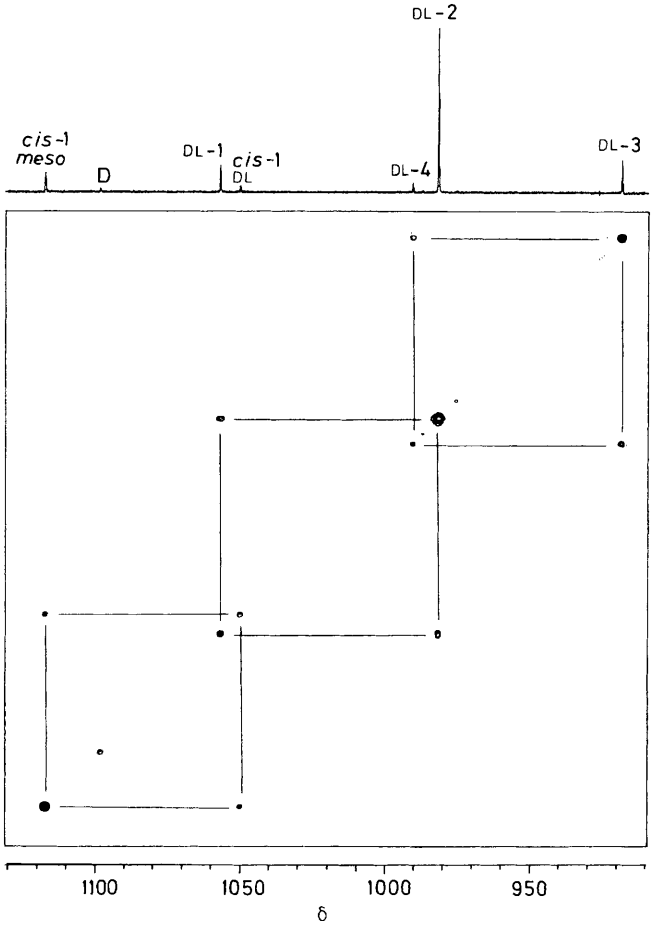

Figure 6. Platinum-195 two-dimensional EXSY spectrum of $[PtIMe_3\{(MeS)_2CHCH(SMe)_2\}]$ at 233 K. At this temperature only the exchanges due to S^2 inversions are visible; D = dinuclear complex

K are shown in Figure 6. Seven signals were detected indicating seven solution species. On raising the temperature, six of these signals showed some exchange broadening whereas the remaining signal (D) remained sharp. A ^{195}Pt two-dimensional EXSY spectrum (Figure 6) identified two sets of exchange processes, one involving four-site exchange and the other a two-site exchange. The conclusions drawn from these experiments were: (*i*) six out of seven possible invertomers were present; (*ii*) four were associated with the *trans* isomer and two with one of the *cis* isomers; and (*iii*) the seventh species (D) was a chemically distinct impurity, and from the 1:8:18:8:1 quintet splitting of its methine ^1H signal was attributed to the dinuclear species (**3**) (Figure 1). Of the two possible *cis* isomers, *cis*-1 was more likely to be favoured on steric grounds. Also, the occurrence of the dinuclear species (**3**) as reaction by-products is thought more likely to be the result of the *cis*-1, rather than the *cis*-2, species, acting as templates for the attachment of a second $PtXMe_3$ moiety.

In the bis(methylthio)ethane complexes $[PtXMe_3(MeSCH_2CH_2SMe)]$ (X = Cl, Br, or I)[2,3] the *meso*-1 invertomers having both co-ordinated S-methyls *cis* to X are the most abundant. In the present tetrakis(methylthio)ethane complexes the contiguous unco-ordinated S-methyls will most clearly prefer to adopt a mutual *trans* relationship and such a relationship may extend to the adjacent co-ordinated S-methyls. Thus, the most abundant invertomer is attributed to DL-2, and the least abundant to DL-4 (Figure 4) where the co-ordinated and unco-ordinated S-methyls eclipse each other. The other DL species may be assigned from the ^{195}Pt two-dimensional EXSY spectra (Figure 6), where the exchanges due to S^2 inversion are clearly shown. (*N.B.* The S^1 isomer rates are too slow to be detected under these particular conditions but were observed in other experiments.) The remaining two ^{195}Pt signals must be associated with the *cis*-1 isomer. These species produce a singlet and an AB quartet (J_{AB} = 4.8 Hz) in the ^1H spectrum and are therefore attributed to *meso*-1 and DL isomers respectively. It is noteworthy that the smaller scalar coupling of this AB quartet compared to those of the other AB quartets (J_{AB} = 11—12 Hz) reflects the *cis* rather than a *trans* disposition of the methine protons.

All six invertomer species can therefore be unambiguously identified, and their ^{195}Pt shifts and relative populations are reported in Table 2. The data exhibit a number of very consistent trends. The ^{195}Pt shifts for all invertomers decrease as the halogen mass/size increases in accordance with previous findings.[17] The Cl–Br change is consistently less than the Br–I change, with values of the ratio Δδ(Cl–Br)/Δδ(Br–I) being in the very narrow range 0.54—0.59 for all six invertomers. The different ^{195}Pt invertomer shifts are not easily rationalised as they clearly depend in a very sensitive manner on the overall anisotropy of the invertomer geometries. The higher-frequency shifts are associated with species having co-ordinated S-methyl *cis* to halogen (*viz.* *trans*/DL-1 and *cis*-1/*meso*-1). These two particular solution species are notable in that their populations decrease appreciably with increasing halogen mass/size while the populations of the other species increase. However, this does not affect the relative ordering of populations as shown below.

$$\underbrace{\text{DL-2} > \text{DL-1} > \text{DL-3} > \text{DL-4}}_{trans} \gg \underbrace{(meso\text{-1} \gg \text{DL})}_{cis\text{-1}}$$

Turning to the methine ^1H spectra, all signals can be unambiguously assigned and full details are given in Figure 5

Table 3. Hydrogen-1 n.m.r. parameters for $[PtXMe_3\{(MeS)_2CHCH(SMe)_2\}]$ (X = Cl, Br, or I); methine region, 213 K

			δ			^3J(H–H)/Hz		
Configuration	Invertomer	$^1H^a$	Cl	Br	I	Cl	Br	I
trans	DL-1	1	4.19	4.10	4.05	11.41	12.51	11.50
		2	3.69	3.59	3.54	11.43	12.50	11.50
	DL-2	3	4.23	4.21	4.27	11.80	12.56	11.90
		4	3.43	3.38	3.37	11.81	12.56	11.90
	DL-3	5	4.46	4.49	4.55	12.03	11.26	11.50
		6	3.66	3.67	3.77	11.75	11.26	11.50
	DL-4	7	4.5[b]	4.52	4.61	12.0[b]	12.00	11.80
		8	3.89	3.81	3.67	11.59	12.00	11.80
cis-1	*meso*-1	9	4.5[b]		4.43			
		10	4.84	4.86	4.93	4.27	4.29	4.30
	DL	11	4.5[b]	4.45	4.39		4.29	4.30

[a] Labelling refers to Figures 3 and 4. [b] Approximately.

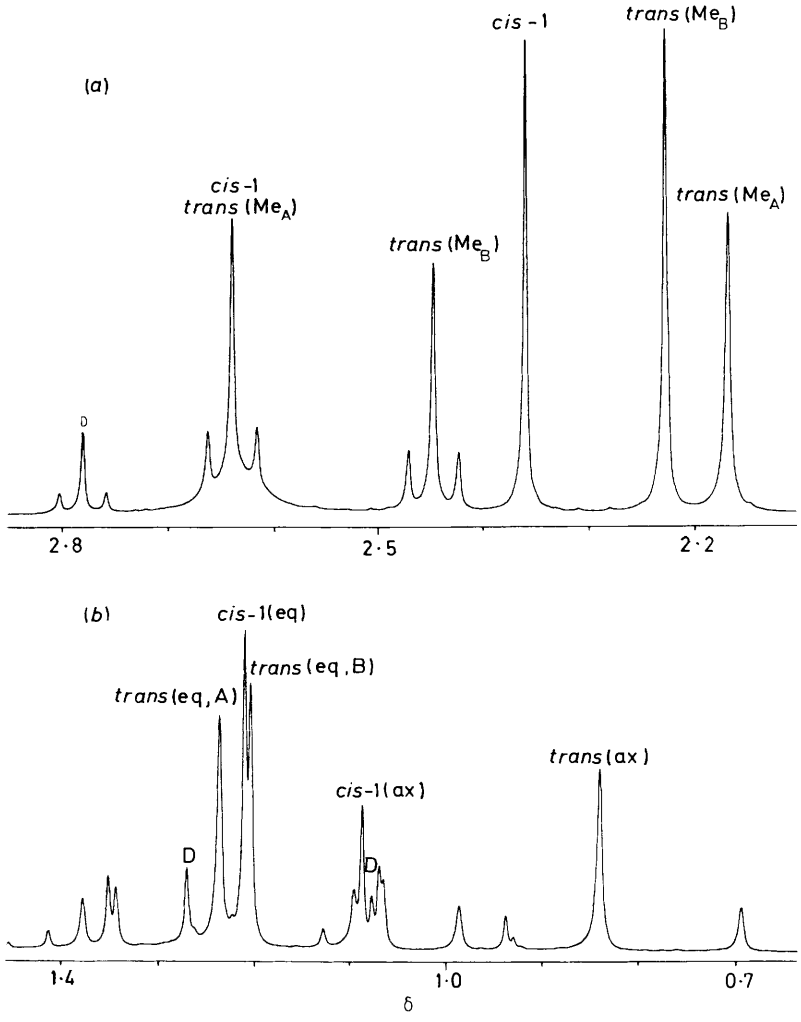

Figure 7. Proton n.m.r. spectrum of $[PtClMe_3\{(MeS)_2CHCH(SMe)_2\}]$ at 333 K showing (*a*) S-methyl signals (co-ordinated and unco-ordinated) and (*b*) Pt-methyl signals. Signal labelling refers to Figure 2. All unlabelled signals in PtMe region are ^{195}Pt satellites; D = dinuclear complex

and Table 3. The signal labelling 1—11 refers to the labelling in Figures 3 and 4. The assignments are based on three general observations. First, methine protons *cis* to X occur at considerably higher frequencies than those *trans* to X, secondly, these hydrogen signals show persistently greater coupling to ^{195}Pt than do the signals of the methines *trans* to X, and thirdly those methines with contiguous *trans* co-ordinated S-methyls occur at higher frequencies than those with *cis* co-ordinated S-methyl neighbours. Thus $\delta(H^5) > \delta(H^3)$, $\delta(H^7) > \delta(H^1)$, $\delta(H^8) > \delta(H^6)$, and $\delta(H^2) > \delta(H^4)$.

On raising the temperature at which the spectra were obtained, the four *trans*-isomer AB quartets collapse to a single

Table 4. Hydrogen-1 n.m.r. parameters for $[PtXMe_3\{(MeS)_2CHCH(SMe)_2\}]$ (X = Cl, Br, or I); methine region, 333 K

Configuration	^1H*	δ Cl	δ Br	δ I	^3J(H–H)/Hz Cl	^3J(H–H)/Hz Br	^3J(H–H)/Hz I
trans	1 3 5 7	4.29	4.30	4.36	11.58	10.01	
	2 4 6 8	3.58	3.43	3.40	11.58	12.15	11.0
cis-1	9 10 11	4.55	4.52	4.54			

* Labelling refers to Figures 3 and 4.

Table 5. Hydrogen-1 n.m.r. parameters for $[PtXMe_3\{(MeS)_2CHCH(SMe)_2\}]$ (X = Cl, Br, I); S-methyl region, 333 K

Configuration	Type S	No.	δ Cl	δ Br	δ I
trans	Co-ord.	S^1	2.62[a]	2.6[a]	2.6[a]
	Co-ord.[b]	S^2	2.45	2.40	2.42
	Unco-ord.	S^2	2.22	2.16	2.17
	Unco-ord.	S^1	2.17	2.11	2.11
cis-1	Co-ord.[c]		2.64	2.64	2.74
	Unco-ord.		2.36	2.29	2.30

[a] Approximately. [b] ^3J(Pt–H) = 11.85 (X = Cl), 12.56 (Br), and 13.18 (I) Hz. [c] ^3J(Pt–H) = 11.67 (Cl), 12.06 (Br), and 13.06 (I) Hz.

exchange-averaged AB quartet, and the singlet plus AB quartet signals of the *cis* isomer average to a singlet with ^{195}Pt satellites. The methine proton data measured at 333 K are given in Table 4.

Sulphur-methyl region. The co-ordinated and unco-ordinated S-methyls are easily distinguished by the signals of the former appearing to higher frequencies of the latter and possessing ^{195}Pt satellites. In the spectra at 333 K where S inversion is fairly rapid this is clearly shown and the assignments are in no doubt (Table 5). In the spectrum of $[PtClMe_3L]$ [Figure 7(*a*)] the signal at *ca.* δ 2.6 is composite, being made up of a sharp signal with ^{195}Pt satellites due to *cis*-1 and a broad signal due to *trans*(co-ordinated Me_A). The greater width of this signal and also that at δ 2.17 [due to *trans*(unco-ordinated Me_A)] is due to residual exchange broadening from the S inversion (see later). On cooling the complexes to arrest the S inversion the spectra become very complex as expected, but by a careful scrutiny of the band-shape changes in the temperature range 333—213 K the major signals of the slow inversion spectra were assigned.

Platinum-methyl region. In this region the Pt-methyls (*trans* X) (*i.e.* axial PtMe) and (*trans* S) (*i.e.* equatorial PtMe) may be clearly distinguished since the former produce signals at lower frequencies to the latter and exhibit ^2J(Pt–H) couplings which, in the case of the chloro- and bromo-complexes, are 1—3 Hz larger than those due to the equatorial Pt-methyls (Table 6). In the fast-inversion limit the assignment of the five signals expected for the two isomers is unambiguous [Table 6, Figure 7(*b*)]. The slow-inversion-limiting spectrum (213 K) due to the six n.m.r.-distinguishable invertomers is less easy to interpret but a tentative assignment for the $[PtClMe_3L]$ complex proved possible.

X-*Ray Crystallography.*—The main conclusion of the low-temperature n.m.r. studies was that the predominant complex species in $CDCl_3$ solvent was the *trans*/DL-2 invertomer, having unco-ordinated S-methyls *trans* to each other and also *trans* to their neighbouring co-ordinated S-methyls.

The result of an *X*-ray crystal analysis of $[PtIMe_3L]$ is shown in Figure 8. This depicts a similar disposition of S-methyl groups in the crystalline state, thus lending support to the

Table 6. Hydrogen-1 n.m.r. parameters for $[PtXMe_3\{(MeS)_2CHCH(SMe)_2\}]$ (X = Cl, Br, or I); Pt-methyl region, 333 K

Configuration	Me *trans* to	δ Cl	δ Br	δ I	^2J(Pt–H)/Hz Cl	^2J(Pt–H)/Hz Br	^2J(Pt–H)/Hz I
trans	X	0.84	0.86	0.99	72.89	72.10	69.69
	S	1.24	1.23	1.41	70.78	70.20	71.53
	S	1.20	1.26	1.38	69.95	71.04	70.81
cis-1	X	1.08	1.11	1.24	74.32	73.51	71.19
	S	1.21	1.24	1.41	70.78	70.93	71.53

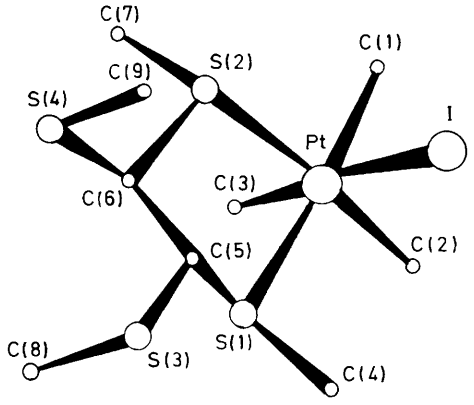

Figure 8. Crystal structure of $[PtIMe_3\{(MeS)_2CHCH(SMe)_2\}]$ showing the atomic labelling

solution n.m.r. arguments. It is noteworthy that for this iodo complex the corresponding solution species (*trans*/DL-2) is *ca.* 55% abundant (Table 2). The molecular dimensions (atomic co-ordinates, bond lengths, and bond angles) of the iodo complex in the solid state are given in Table 7. The five-membered ring is puckered with the C(5) atom 0.85 Å from the least-squares best plane through the other four atoms [Pt, S(1), S(2), and C(6)] which themselves deviate by *ca.* 0.04 Å from the plane. The mean Pt–C, Pt–I, Pt–S, and C–S distances of 2.04(4), 2.800(2), 2.433(8), and 1.82(3) Å respectively are all within the range of expected values. The bond angles I–Pt–S(1) and I–Pt–S(2) show that the ring is puckered such that S(2) is towards the halogen side of the structure and S(1) is away from the halogen. This distortion enables the co-ordinated S-methyls to be more easily accommodated.

Dynamic N.M.R. Studies.—The methine regions of the ^1H spectra were most tractable for dynamic n.m.r. studies since the spectra in the slow- and fast-exchange limits could be firmly interpreted. Inversion within the *trans* species was considered first. Each *trans*/DL invertomer produces an AB quartet of lines with ^{195}Pt satellites. These are interconverted by inversion of the co-ordinated S atoms according to the dynamic spin system shown below. The labelling of the methine protons is according

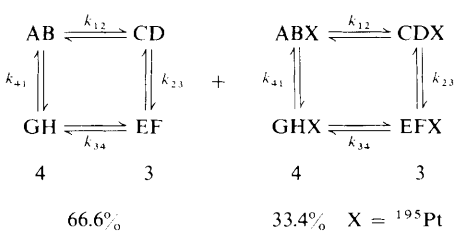

Table 7. Atomic parameters ($\times 10^4$), bond lengths (Å) and bond angles (°) of $[PtIMe_3\{(MeS)_2CHCH(SMe)_2\}]$

Atom	*X/a*	*Y/b*	*Z/c*
Pt	8 310(2)	1 863(1)	5 322(1)
I	6 728(3)	2 805(1)	3 796(1)
S(1)	10 795(9)	2 861(4)	5 749(4)
S(2)	6 565(11)	2 764(5)	6 211(5)
S(3)	10 849(11)	4 708(4)	6 201(5)
S(4)	7 242(12)	4 390(5)	7 219(6)
C(1)	6 210(56)	993(20)	5 095(30)
C(2)	9 881(47)	1 199(21)	4 680(30)
C(3)	9 491(52)	1 128(21)	6 423(20)
C(4)	11 782(64)	3 194(19)	4 766(25)
C(5)	9 446(35)	3 795(15)	5 966(18)
C(6)	8 323(35)	3 532(15)	6 700(18)
C(7)	6 030(53)	2 288(22)	7 248(22)
C(8)	12 079(49)	4 499(20)	7 330(20)
C(9)	5 945(56)	4 883(21)	6 187(31)

Pt–I	2.800(2)	S(2)–C(6)	1.846(26)
Pt–S(1)	2.427(7)	S(2)–C(7)	1.805(37)
Pt–S(2)	2.438(8)	S(3)–C(5)	1.787(26)
Pt–C(1)	2.069(39)	S(3)–C(8)	1.797(34)
Pt–C(2)	1.986(35)	S(4)–C(6)	1.811(27)
Pt–C(3)	2.084(33)	S(4)–C(9)	1.842(42)
S(1)–C(4)	1.803(39)	S(5)–C(6)	1.522(36)
S(1)–C(5)	1.848(26)		
S(1)–Pt–S(2)	85.2(2)	Pt–S(1)–C(4)	111.6(13)
I–Pt–C(1)	91.3(11)	Pt–S(1)–C(5)	99.8(8)
I–Pt–C(2)	95.6(10)	C(4)–S(1)–C(5)	101.3(15)
I–Pt–C(3)	177.6(9)	Pt–S(2)–C(6)	101.8(9)
I–Pt–S(1)	93.5(2)	Pt–S(2)–C(7)	114.3(12)
I–Pt–S(2)	86.1(2)	C(6)–S(2)–C(7)	100.5(14)
C(1)–Pt–S(1)	174.4(11)	S(1)–C(5)–S(3)	112.6(13)
C(1)–Pt–S(2)	92.3(11)	S(1)–C(5)–C(6)	105.4(17)
C(1)–Pt–C(2)	91.6(15)	S(3)–C(5)–C(6)	116.6(18)
C(1)–Pt–C(3)	87.4(14)	C(5)–S(3)–C(8)	102.7(14)
C(2)–Pt–S(1)	90.8(10)	C(5)–C(6)–S(2)	109.3(17)
C(2)–Pt–S(2)	175.7(10)	S(2)–C(6)–S(4)	109.9(14)
C(2)–Pt–S(3)	82.4(14)	C(5)–C(6)–S(4)	114.5(18)
C(3)–Pt–S(1)	88.0(9)	C(6)–S(4)–C(9)	100.3(16)
C(3)–Pt–S(2)	96.0(9)		

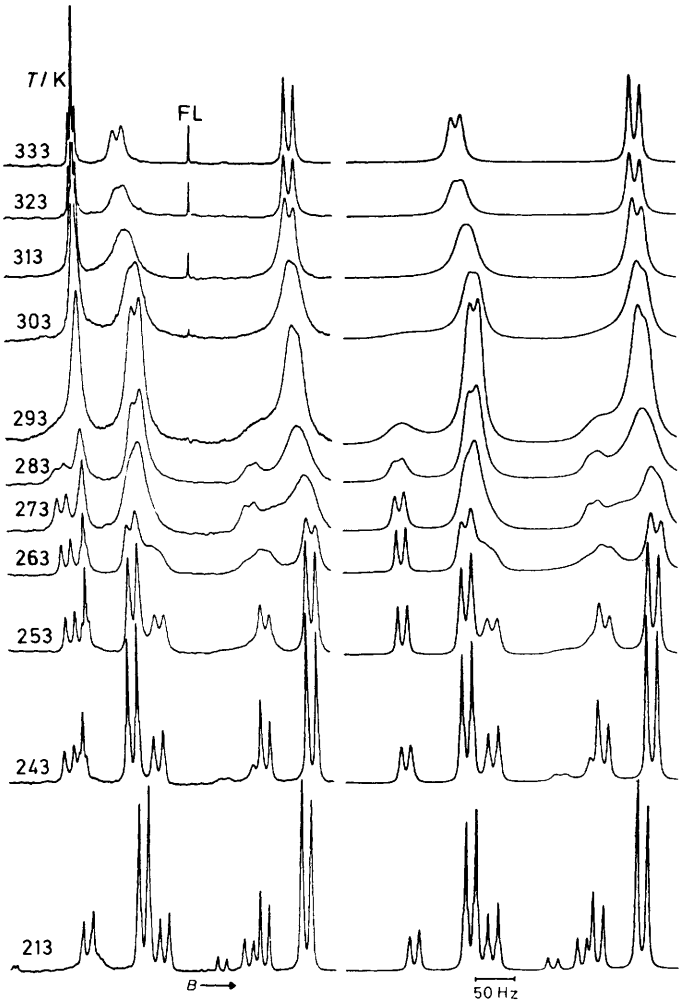

Figure 9. Experimental (left) and computer-simulated (right) spectra of the methine proton region of $[PtBrMe_3\{(MeS)_2CHCH(SMe)_2\}]$, showing the effects of pyramidal sulphur inversion. See Tables 3 and 4 for the signal assignments and Table 8 for the rate data; FL = free ligand

to Figure 3. Synchronous double inversion of S atom pairs is known to be negligibly slow for chelate systems of this type,[15] and thus only rate constants relating adjacent configurations in these schemes need be considered. Reverse rate constants to the ones shown are given by equilibrium relationships $p_i k_{ij} = p_j k_{ji}$ where p_i and p_j are the populations of the configurations i and j. Initially, bandshape fitting was performed with all forward rate constants made equal, but this formulation did not reproduce the experimental band shapes satisfactorily. As there appeared to be evidence of markedly different rates of inversion of the two sulphur donors, the dynamic problem was reformulated using three independent rate constants, two parameters k_{12} and k_{34} describing inversion at S^2 and a single magnitude of rate constant k_{14} ($=k_{23}$) describing inversion at S^1. The number of independent rate constants was restricted to three to aid the practicality of the fitting procedure, since it would have been very difficult to achieve *unique* fittings of simulated spectra based on four rate values. In any case this three-rate fitting basis is considered a very good approximation since S^1 inversion only becomes appreciable at temperatures when S^2 inversion is quite rapid and there is little n.m.r. distinction between the invertomer pairs DL-1 and DL-2, or DL-3 and DL-4. Furthermore, the relatively low populations of DL-3 and DL-4 tend to make the ^1H spectra rather insensitive to the rate constant for S^1 inversion.

This three-rate constant formulism produced extremely good visual matchings of experimental and theoretical spectra. The case of $[PtBrMe_3L]$ is shown in Figure 9, and the 'best-fit' values for all three complexes in Table 8. In addition to the temperature dependence of the rate constants, allowances had to be made for significant temperature dependences of the chemical shifts and invertomer populations. Over the temperature range 243—333 K, the latter changed such that the DL-2 population decreased by *ca.* 20% and the other populations proportionately increased. It will be seen from Table 8 that at temperatures $< ca.$ 273 K the S^1 inversion rate is extremely slow and the spectra are sensitive mainly to k_{12} and k_{34}. This is clearly reflected in the changes in lineshape of the high-frequency component of the intense AB quartet of the DL-2 species (Figure 9). On raising the temperature from 213 K this signal starts broadening to an extent that by 273 K the vicinal H–H coupling is obscured. Above that temperature, however, the signal sharpens to reveal this coupling again at 293 K. Above this temperature, however, the effect of S^1 inversion is apparent as the signal broadens again and eventually forms the higher-frequency component of the fast inversion-averaged methine quartet at 333 K. The simulated spectra reproduce these subtle changes very precisely and thus the sets of rate constants given in Table 8 are considered to be of high accuracy.

Simulation of pyramidal inversion in the *cis*-1 isomer is in theory a much simpler problem as it produces exchange of the methine environments of the two species *meso*-1 and DL. The dynamic spin problem is simply $AA' \underset{k_{21}}{\overset{k_{12}}{\rightleftharpoons}} BC$ where the labelling refers to Figure 4 and ^{195}Pt satellite signals are neglected. In practice, bandshape fittings were hampered by the low intensity of the DL signals and the near overlap of the low-frequency DL doublet with the *meso*-1 signal (Table 3). However, approximate band-shape analysis in the range 233—263 K was possible for the bromo complex and best-fit rate constants for the *meso*-1 ⟶ DL exchange obtained (Table 9). A similar analysis was not possible for the chloro complex on account of the very low abundance of the DL species (Table 2). For the iodo complex, quantitative ^{195}Pt two-dimensional EXSY experiments[15] were performed over a limited range of temperatures and reliable rate data obtained (Table 9).

Table 8. Variable-temperature rate constants for sulphur inversion in the *trans* isomer of $[PtXMe_3L]$ (X = Cl, Br, or I)

	k_{12}/s^{-1}			k_{34}/s^{-1}			$k_{14}(=k_{23})/s^{-1}$		
T/K	Cl	Br	I	Cl	Br	I	Cl	Br	I
243	5	5	4	20	14	4	0	0	0
253	15	20	15	50	45	17	0	0	0
263	42	50	35	105	86	40	0	1	2
273	85	110	95	200	300	180	3	4	4
283	240	200	230	400	600	300	10	10	8
293	500	470	550	800	1 200	700	25	25	15
303	1 600	950	1 200	1 800	2 550	1 500	55	50	32
313	3 200	1 900	2 500	3 500	4 900	3 500	120	140	65
323	6 400	3 850	6 000	7 000	10 400	7 500	255	320	160
333		6 650	12 000		19 000	16 000		600	320

Table 9. Variable-temperature rate constants for sulphur inversion in the *cis* isomer of $[PtXMe_3L]$ (X = Br or I)

	k_{12}/s^{-1}	
T/K	Br[a]	I[b]
223		0.13
233	4	0.64
243	8	2.01
253	20	
263	50	

[a] Values from ^1H one-dimensional band-shape analysis. [b] Values from ^{195}Pt two-dimensional EXSY spectra.

Discussion

The foregoing bandshape analysis of the methine regions of the ^1H spectra of the complexes $[PtXMe_3L]$ (X = Cl, Br, or I) provided rate constant data covering a wide temperature range, thus enabling activation energies from the sulphur inversions to be calculated using both Arrhenius and Eyring rate theories. The full sets of energy data for the *trans* and *cis*-1 isomers are contained in Tables 10 and 11, respectively. The data for S^2 inversion are considered more reliable than for S^1 inversion (for reasons mentioned earlier), and no mechanistic significance is attached to the $\Delta S^\ddagger$ values which are not close to zero. The majority of the $\log_{10}(A/s^{-1})$ values are around 13, implying a purely intramolecular inversion mechanism. All the $\Delta G^\ddagger$ values refer to 298.15 K and certain clear trends are apparent. The most important and striking is the difference in the activation energies of the two sulphurs in the *trans* configuration. Values for S^2 inversion are in the range 54—56 kJ mol^{-1} and for S^1 inversion in the range 64.0—64.8 kJ mol^{-1}. Thus, the pyramidal inversion energy of the sulphur atom S^2 with a contiguous S-methyl *cis* to X is *ca.* 9 kJ mol^{-1} lower than that of the S atom S^1 with a contiguous S-methyl *trans* to X. For a given temperature such an energy difference corresponds to S^2 inverting *ca.* 40—50 times more rapidly than S^1. Such a difference must be reflected in the different strengths of the Pt–S^1 and Pt–S^2 bonds due to the different relationships of the two unco-ordinated S-methyls to the axial substituents on the Pt atom. Clear evidence for the Pt–S^2 bond being slightly weaker than the Pt–S^1 bond is contained in the *X*-ray data of the iodo complex, where the lengths of these bonds are 2.438 and 2.427 Å respectively.

The inversion energies for the *cis*-1 isomers lie between the values for S^1 and S^2 inversion in the *trans* isomers, probably reflecting the fact that in the *cis*-1 species, n.m.r. bandshape analysis cannot distinguish between S^1 and S^2 inversions in the absence of any *meso*-2 species.

The $\Delta G^\ddagger$ values for both the *trans* and *cis*-1 isomers show no

Table 10. Activation parameters for the sulphur inversion process in $[PtXMe_3\{(MeS)_2CHCH(SMe)_2\}]$ (X = Cl, Br, or I)

X	Exchange	Inversion	E_a/kJ mol^{-1}	$\log_{10}(A/s^{-1})$	$\Delta H^\ddagger$/kJ mol^{-1}	$\Delta S^\ddagger$/J K^{-1} mol^{-1}	$\Delta G^\ddagger$/kJ mol^{-1}
Cl	DL-1 ⟶ DL-2	S^2	57.97 ± 1.07	13.13 ± 0.2	55.7 ± 1.04	−1.2 ± 3.8	56.05 ± 0.09
	DL-3 ⟶ DL-4	S^2	47.39 ± 0.98	11.43 ± 0.19	45.11 ± 0.96	−33.8 ± 3.5	55.20 ± 0.09
	DL-1 ⟶ DL-4	S^1	72.85 ± 9.79	14.25 ± 1.71	70.35 ± 9.8	19.4 ± 32.8	64.56 ± 0.01
	DL-2 ⟶ DL-3						
Br	DL-1 ⟶ DL-2	S^2	52.17 ± 0.94	12.00 ± 0.17	49.81 ± 0.94	−23.2 ± 3.3	56.73 ± 0.05
	DL-3 ⟶ DL-4	S^2	53.47 ± 0.81	12.64 ± 0.15	51.11 ± 0.80	−10.8 ± 2.8	54.34 ± 0.04
	DL-1 ⟶ DL-4	S^1	65.52 ± 1.32	13.07 ± 0.23	63.07 ± 1.32	−3.0 ± 4.5	63.95 ± 0.01
	DL-2 ⟶ DL-3						
I	DL-1 ⟶ DL-2	S^2	58.92 ± 0.72	13.27 ± 0.13	56.57 ± 0.7	1.2 ± 2.5	56.22 ± 0.04
	DL-3 ⟶ DL-4	S^2	60.31 ± 1.25	13.63 ± 0.23	57.96 ± 1.26	8.1 ± 4.4	55.54 ± 0.06
	DL-1 ⟶ DL-4	S^1	52.71 ± 2.24	10.67 ± 0.4	50.25 ± 2.21	−48.9 ± 7.5	64.83 ± 0.02
	DL-2 ⟶ DL-3						

Table 11. Activation parameters for the sulphur inversion process in *cis*-1 $[PtXMe_3\{(MeS)_2CHCH(SMe)_2\}]$ (X = Br or I)*

X	Exchange	E_a/kJ mol^{-1}	$\log_{10}(A/s^{-1})$	$\Delta H^\ddagger$/kJ mol^{-1}	$\Delta S^\ddagger$/J K^{-1} mol^{-1}	$\Delta G^\ddagger$/kJ mol^{-1}
Br	*meso*-1 ⟶ DL	43.13 ± 3.02	10.23 ± 0.64	41.08 ± 2.99	−55.8 ± 12.1	57.73 ± 0.62
I	*meso*-1 ⟶ DL	61.24 ± 4.00	13.49 ± 0.9	59.31 ± 4.03	7.1 ± 17.3	57.19 ± 1.14

* Data not available for chloro complex due to unfavourable invertomer populations and overlapping chemical shifts.

Table 12. Comparison of differences in ground-state energies (ΔG°) and transition-state energies ($\Delta G^{\ddagger}$) for the *trans* isomer of [$PtBrMe_3$-{$(MeS)_2CHCH(SMe)_2$}]

Process	$\Delta G^{\ddagger}$(213 K)/ kJ mol^{-1}	$\Delta\Delta G^{\ddagger}$/ kJ mol^{-1}	$\Delta\Delta G^{\circ}$(213 K)/ kJ mol^{-1}
DL-1 ⟶ DL-2	54.75		
		−8.96	−1.65[a]
DL-2 ⟶ DL-3	63.71		
		10.30	3.04[b]
DL-3 ⟶ DL-4	53.41		
			1.59[c]
DL-4 ⟶ DL-1	*d*		

[a] $-RT\ln[p(\text{DL-1})/p(\text{DL-2})]$. [b] $-RT\ln[p(\text{DL-2})/p(\text{DL-3})]$. [c] $-RT\ln[p(\text{DL-3})/p(\text{DL-4})]$. [d] Not measured.

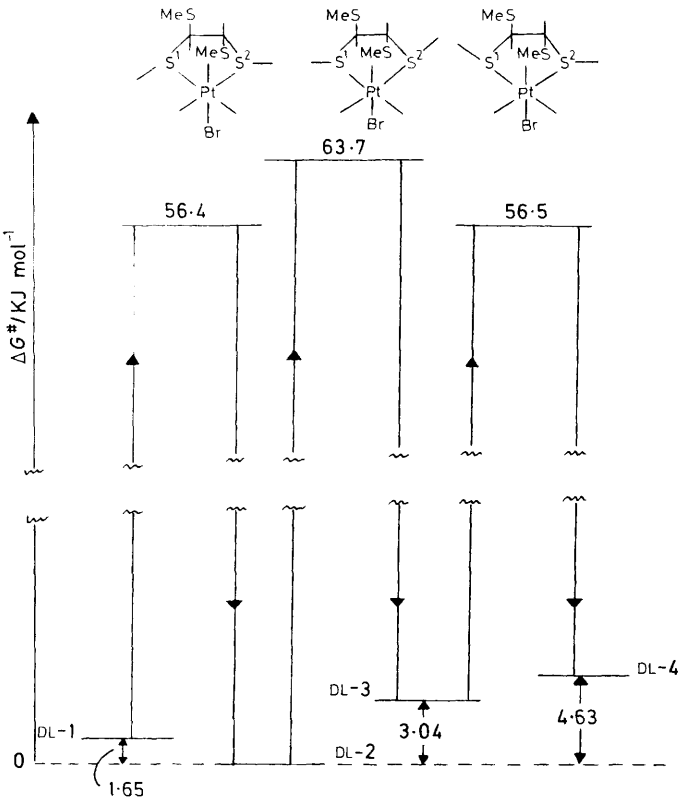

Figure 10. Activation energy ($\Delta G^{\ddagger}$) profile for pyramidal sulphur inversion in [$PtBrMe_3${$(MeS)_2CHCH(SMe)_2$}] showing the relative ground-state and transition-state energies

significant dependences on the nature of the halogen as is usual in such *cis* chelate complexes.[1]

In the case of the *trans* isomers, the different $\Delta G^{\ddagger}$ values for the inversion processes may be wholly or partly due to the difference in ground-state energies of the four DL invertomers. These may be expressed as ΔG° data, where $\Delta G^{\circ} = -RT\ln K^{\circ}$ and $K^{\circ} = p_i/p_j$, the ratio of pairs of invertomer populations. The values are listed in Table 12 and should be compared with the differences in the $\Delta G^{\ddagger}$ values for consecutive interconversions (*e.g.* DL-1 ⟶ DL-2, and DL-2 ⟶ DL-3). All these data have been used to produce a pyramidal energy profile for the complex [$PtBrMe_3L$] (Figure 10). It will be seen that the transition-state intermediates for the two S^2 inversions, *viz.* DL-1 ⟶ DL-2 and DL-3 ⟶ DL-4, have almost identical energies. This is not surprising since they differ only in the relationships of the S^1-methyl and its contiguous unco-ordinated S-methyl *trans* to X. That such an interaction is negligible may be deduced from $\Delta G^{\ddagger}$ data measured earlier[3] for the bis(methylthio)ethane complexes, [$PtXMe_3(MeSCH_2CH_2SMe)$] (X = Cl, Br, or I). These fall in the range 62.6–63.3 kJ mol^{-1}, no distinction being made between S^1 and S^2 inversion. Thus, the presence of an unco-ordinated S-methyl substituent on the ligand backbone *cis* to halogen appears to accelerate the pyramidal inversion of the contiguous S-methyl by weakening the Pt–S^2 bond, whereas an unco-ordinated S-methyl *trans* to halogen has no appreciable effect on the inversion characteristics of its neighbouring S^1 atom.

The energy profile (Figure 10) does show, however, that the intermediate associated with the S^1 inversion, DL-2 ⟶ DL-3, is *ca.* 7 kJ mol^{-1} higher in energy than the other intermediates.

These pyramidal inversion fluxions are only a prelude to more extensive, higher-temperature fluxionality in these complexes. This will be the subject of a later paper.

References

1 E. W. Abel, S. K. Bhargava, and K. G. Orrell, *Prog. Inorg. Chem.*, 1984, **32**, 1.
2 E. W. Abel, A. R. Khan, K. Kite, K. G. Orrell, and V. Šik, *J. Chem. Soc., Dalton Trans.*, 1980, 1169.
3 E. W. Abel, A. R. Khan, K. Kite, K. G. Orrell, and V. Šik, *J. Chem. Soc., Dalton Trans.*, 1980, 1175.
4 E. W. Abel, S. L. Bhargava, K. Kite, K. G. Orrell, V. Šik, and B. L. Williams, *J. Chem. Soc., Dalton Trans.*, 1982, 583.
5 E. W. Abel, A. R. Khan, K. Kite, K. G. Orrell, and V. Šik, *J. Chem. Soc., Dalton Trans.*, 1980, 2208.
6 E. W. Abel, A. R. Khan, K. Kite, K. G. Orrell, and V. Šik, *J. Chem. Soc., Dalton Trans.*, 1980, 2220.
7 E. W. Abel, K. Kite, K. G. Orrell, V. Šik, and B. L. Williams, *J. Chem. Soc., Dalton Trans.*, 1981, 2439.
8 E. W. Abel, T. E. MacKenzie, K. G. Orrell, and V. Šik, *J. Chem. Soc., Dalton Trans.*, 1986, 2173.
9 M. F. Lappert, D. B. Shaw, and G. M. McLaughlin, *J. Chem. Soc., Dalton Trans.*, 1979, 427.
10 B. Cetinkaya, P. B. Hitchcock, M. F. Lappert, P. L. Pye, and D. B. Shaw, *J. Chem. Soc., Dalton Trans.*, 1979, 434.
11 E. W. Abel, K. Kite, and B. L. Williams, *J. Chem. Soc., Dalton Trans.*, 1983, 1017.
12 D. Seebach and A. K. Beck, *Chem. Ber.*, 1982, **105**, 3892.
13 E. W. Abel, K. M. Higgins, K. G. Orrell, V. Šik, E. H. Curzon, and O. W. Howarth, *J. Chem. Soc., Dalton Trans.*, 1985, 2195.
14 D. A. Kleier and G. Binsch, Program 165, Quantum Chemistry Program Exchange, Indiana University, 1970.
15 E. W. Abel, T. P. J. Coston, K. G. Orrell, V. Šik, and D. Stephenson, *J. Magn. Reson.*, 1986, **70**, 34.
16 G. M. Sheldrick, SHELX Systems Report, University of Cambridge, 1976.
17 P. S. Pregosin, *Annu. Rep. NMR Spectrosc.*, 1986, **17**, 285.

Received 3rd *May* 1988; *Paper* 8/01712C